

Development and Characterization of Amorphous Nanofiber Drug Dispersions Prepared Using Pressurized Gyration

Bahijja Tolulope Raimi-Abraham,[†] Suntharavathanan Mahalingam,[‡] Philip J. Davies,[§] Mohan Edirisinghe,[‡] and Duncan Q. M. Craig*,[†]

[†]University College London School of Pharmacy, 29-39 Brunswick Square, London, WC1N 1AX, U.K.

[‡]Department of Mechanical Engineering, University College London, Torrington Place, London, WC1E 7JE, U.K.

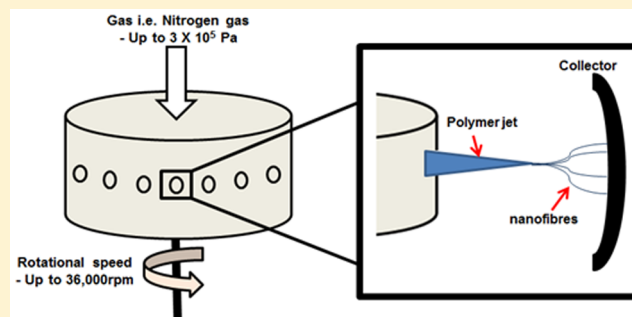
[§]TA Instruments—A Division of Waters U.K., 730-740 Centennial Court, Centennial Park, Elstree, Hertfordshire, WD6 3SZ, U.K.

S Supporting Information

ABSTRACT: Nanofibrous systems are attracting increasing interest as a means of drug delivery, although a significant limitation to this approach has been manufacture on a scale commensurate with dosage form production. However, recent work has suggested that nanofibers may be successfully manufactured on a suitable scale using the novel process of pressurized gyration (PG). In this study, we explore the potential of PG as a novel means of generating amorphous solid dispersions of poorly water-soluble drugs with enhanced dissolution performance. We examine the effect of increasing drug loading on fiber properties including size, surface characteristics, and the physical state of both components.

Dispersions of ibuprofen in poly(vinylpyrrolidone) (PVP) were prepared (up to 50% w/w loading) and characterized using a range of imaging, thermal, diffraction, and spectroscopic techniques, while the release profiles were studied using sink and non-sink (pH 1.0) conditions. The drug was found to be dispersed on a molecular basis within the fibers; attenuated total reflection FTIR indicated evidence for a direct interaction between the drug and polymer at lower drug loading by the identification of a strong single band in the carbonyl region and amide region of ibuprofen and PVP respectively. Dissolution studies under sink conditions indicated a substantial increase in release rate, while non-sink studies showed evidence for supersaturation. It is concluded that PG presents a viable method for the production of drug-loaded nanofibers for oral administration with enhanced *in vitro* dissolution rate enhancement.

KEYWORDS: solid dispersion, amorphous, pressurized gyration, PVP, supersaturation, ibuprofen



INTRODUCTION

It is now well established that improving the dissolution properties of Biopharmaceutics Classification System (BCS) class II and IV drugs may significantly improve their oral bioavailability, with low aqueous solubility being a critical factor to be overcome via appropriate formulation. Several formulation strategies have been employed to enhance the oral bioavailability of such drugs including the use of prodrugs,¹ cocrystals,² nanodrugs,³ and solid dispersions (SD).⁴ A SD can be described as a dosage form whereby the drug is dispersed in a biologically inert (usually) polymeric matrix, usually via a liquid intermediate.⁵ Several techniques are available to generate amorphous SDs, the most common at present being hot melt extrusion (HME),^{6,7} with other techniques such as spray drying⁸ and spin-coated films⁹ having also been successfully utilized. Such systems are typically amorphous in nature, with the drug often being present as a molecular dispersion with concomitant issues regarding stability and phase separation.

More recently, fiber-based SDs have been generated using solvent-based nanofabrication methods. Polymeric nanofibers have an extremely high surface-to-volume ratio¹⁰ which may be expected to exert a strong influence on the bioavailability of poorly water-soluble drugs as increasing surface area may increase the dissolution rate.¹¹ These properties make nanofibers attractive for oral drug delivery applications, although little work has been performed to date in this regard.^{12,13} A new solvent-based nanofabrication system, pressurized gyration (PG), has recently been developed by Mahalingam and Edirisinghe.¹⁴ The PG process exploits both simultaneous centrifugal spinning and solution blowing to generate uniform polymeric nanofibers (60–1000 nm).¹⁴ This approach has the potential to produce 6 kg of fiber/h¹⁴ and therefore offers promising mass production capabilities compared to other

Received: February 10, 2015

Revised: September 6, 2015

Accepted: September 24, 2015

Published: September 24, 2015

established polymer nanofiber generation methods such as electrospinning (produces fibers at ca. 0.17 kg/h).¹⁵

The PG system essentially consists of a rotary aluminum vessel containing a series of orifices with dimensions of 0.5 mm on its circumference (Figure 1). The volume of the aluminum

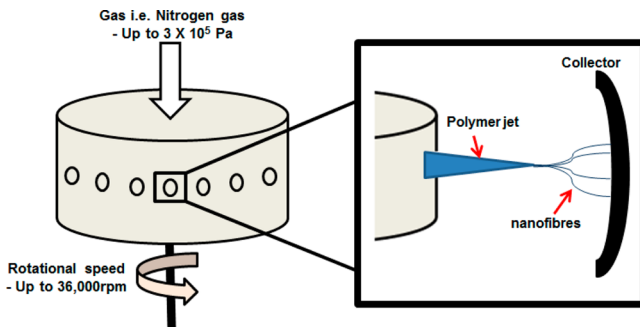


Figure 1. Schematic of the pressurized gyration system, showing the perforated chamber and (inset) the ejection of the polymer jet and associated nanofiber formation.

vessel and the shape of the orifices can be varied to suit the fiber dimensional requirements. The rotating speed of the vessel is controlled by a bidirectional regulator, and motor speeds can go up to 36,000 rpm. The top end of the vessel is connected to a pressurized gas cylinder capable of producing pressures up to 0.3 MPa.

Fiber formation using this technique is explained by Rayleigh–Taylor (RT) instability of the polymer solution jet emerging from the PG vessel orifice.¹⁴ Here, the instability of an interface between two fluids of different densities (in this case the polymer solution and air) occurs where the lighter fluid is applying force to the heavier fluid. In the equilibrium state prior to any perturbation to the system (in the case of PG, prior to the combined influence of centrifugal spinning and solution blowing), the external driving force as the polymer droplet emerges from the vessel orifice is the gravitational force. A surface tension gradient along the polymer liquid–air interface occurs, separating the droplet from the surrounding air. Marangoni stress (mass transfer along an interface between two fluids due to a surface tension gradient) occurs as a result of the surface tension gradient generated inducing a flow to the tip of the polymer droplet.¹⁶ By equating the destabilizing gravitational force per unit volume to the stabilizing surface tension per unit volume, it is possible to determine the instability between the polymer liquid–air interface using eq 1.¹⁷

$$pg \frac{\delta h}{\delta x} = \gamma \frac{\delta^3 h}{\delta x^3} \quad (1)$$

where g is the gravitational force, p the density of the polymer solution, γ the liquid–air surface tension, h the height of the liquid drop hanging under the horizontal surface, and x the vertical distance. During the PG process (i.e., simultaneous centrifugal spinning and solution-gas blowing), the length scale L of the RT instability can be described using eq 2.¹⁷

$$L = \left[\frac{h\gamma}{(p\omega^2 R) + \Delta p} \right]^{1/3} \quad (2)$$

where $(p\omega^2 R)$ is the destabilizing centrifugal force, Δp the pressure difference at the orifice, ω the rotational speed, and R the radius of the vessel.¹⁴

Fiber formation in the PG process occurs in three main steps. A polymer jet initially emerges from the orifice on the face of the vessel, which further stretches (due to $p\omega^2 R$ and Δp), and rapid solvent evaporation occurs, resulting in thinning of the fibers formed.¹⁴ As with most nanofabrication methods, the PG process is governed and influenced by solution parameters (i.e., viscosity, surface tension, polymer molecular weight, and concentration), processing parameters (i.e., pressure and rotational speed), and ambient parameters (i.e., environmental temperature and relative humidity).^{10,14}

In our previous work,¹⁸ the effects of increasing poly(*N*-vinylpyrrolidone) (PVP) molecular weight (M_w) and polymer concentration (% w/v) on fiber formation and fiber characteristics were explored with the identification of minimum values for both parameters resulting in successful nanofiber formation (470–970 nm range).¹⁸ In the study presented here, dispersions of ibuprofen (BCS II) in PVP were prepared (up to 50% w/v loading) and the effect of increasing ibuprofen concentration on fiber solid-state characteristics and the drug release profiles (under sink and non-sink (pH 1) conditions) were investigated. In this manner it is intended that the study will, in the first instance, describe the first use of pressure gyration to manufacture drug-loaded nanofibers and, second, will explore the properties and performance of nanofibers intended for oral delivery, particular using a manufacturing approach that has the potential for much larger scale production.

MATERIALS AND METHODS

Materials. Ibuprofen ($M_w = 206.28 \text{ g mol}^{-1}$, $pK_a = 4.9$,¹⁹ $\log P = 3.97$,¹⁹ aqueous solubility (phosphate buffer at pH 7.2 = 5.2 mg/mL (at 37 °C)))²⁰ and PVP ($M_w = 100,000–150,000 \text{ g mol}^{-1}$, soluble in water and organic solvents)²¹ were kindly donated by BASF (Ludwigshafen, Germany). Ibuprofen 25 (IBU) and Kollidon 90F (K90F) were used in this study. Absolute ethanol (99.8%) analytical grade was obtained from Fischer Scientific, U.K. 0.1 M hydrochloric acid (HCl), pH 1 was prepared with hydrochloric acid 1.16 (32% v/v) analytical grade (Fisher Scientific, U.K.) and distilled water (in-house system).

Methods. Drug–Polymer Miscibility. The solubility parameter, δ , was initially proposed by Hildebrand²² in 1936 as a systemic description of the miscibility behavior between solvents. An extension of δ was further developed by Hansen,²³ who took into account the relative miscibility of polar, dispersion, and hydrogen bonding of systems. In this study, the Hansen solubility parameters, δ , of IBU and K90F were calculated using the functional group contributions for IBU and K90F according to the van Krevelen and Hoflyzer method (eqs 3 and 4).²⁴ The total solubility parameter (δ_t) was determined from the interactions between dispersion forces (δ_d), polar interactions (δ_p), and hydrogen bonding (δ_h) of the functional groups in the molecule divided by the molar volume, V . The units of the solubility parameters are MPa^{1/2}.

$$\delta^2 = \delta_d^2 + \delta_p^2 + \delta_h^2 \quad (3)$$

$$\delta = \sqrt{\left(\frac{\sum F_{di}}{V}\right)^2 \left(\frac{\sqrt{\sum F_{pi}^2}}{V}\right)^2 + \left(\frac{\sqrt{\sum E_{hi}}}{V}\right)^2} \quad (4)$$

where F_{di} , F_{pi} , and E_{hi} are functional group contributions for the dispersion forces, polar interactions, and hydrogen bonding of structural groups reported in the literature at 25 °C.²⁴

The drug–polymer interaction parameter, χ , can be estimated using the difference between the drug (i.e., IBU) and polymer (i.e., K90F) solubility parameters as shown in eq 5.²⁴

$$\chi = \frac{V_0}{RT} (\delta_{\text{drug}} - \delta_{\text{polymer}})^2 \quad (5)$$

where V_0 is the volume of the lattice site, R is the gas constant, and T is the absolute temperature. It is important to note that the interaction parameter, χ , is not constant but temperature and composition dependent.^{25,26}

Sample Preparation. IBU and K90F particles were dry sieved through a 250 µm aperture sieve with a steel mesh (Endecotts LTD, U.K.). Physical mixtures (PMs) with an IBU ratio of 10%, 30%, and 50% w/w were prepared in triplicate. IBU and K90F were codissolved in ethanol. K90F concentration was fixed at 10% w/v while IBU concentration was adjusted to 10%, 30%, and 50% w/v of K90F concentration. Fibers produced will be referred to as IBU-K90F 10%, 30%, and 50% where applicable. K90F and IBU-K90F solutions were mechanically stirred for 2 to 24 h to obtain homogeneous systems. IBU concentration ranges were chosen to establish the effects of these parameters on fiber physicochemical and dissolution characteristics.

Fibers were generated using the PG Mark I device developed by Mahalingam and Edirisinha, capable of producing fibers at 6 kg/h.¹⁴ All experiments were conducted at a fixed rotating speed of 24,000 rpm and at a working pressure of 2.0×10^4 Pa using nitrogen gas; these parameters were selected based on previous optimization studies.¹⁸ The rotational speed influences the fiber length while the working pressure reduces the mean fiber diameter.^{14,18} Here, we maintained constant working parameters so as to investigate the influence of drug loading in isolation, although obviously further optimization is possible.

Characterization of Polymer Solutions. Solution viscosity was measured using an AR1000-N Rheolyst Rheometer (TA Instruments, U.K.). Solution surface tension measurements were measured on a Krüss digital tensiometer K9 using the standard Wilhelmy plate method. All equipment was calibrated before use, and all experiments were conducted at ambient temperature (~25 °C).

Fiber Characterization. Morphological, structural (physical and molecular), and thermal characterization of K90F and K90F-IBU fibers produced was investigated using the following techniques and compared to starting materials and PMs.

Scanning Electron Microscopy (SEM). Fiber morphology and diameter were analyzed using a FEI Quanta 200F field emission scanning electron microscope (SEM). Samples were coated with 20 nm of gold under vacuum using a Quorum Q150T Turbo-Pumped sputter coater with a film thickness monitor unit. All micrographs were taken at an acceleration voltage of 5 kV. The average diameter of the fibers as well as the percentage frequency was determined from the mean value of 100 measurements collected by analyzing the SEM micrographs using ImageJ (USA, version 1.46r).

X-ray Powder Diffraction (XRPD). Structural characterization of fibers produced was conducted using a D/Max-BR diffractometer (RigaKu, Tokyo, Japan) with Cu K α radiation operating at 40 mV and 30 mA over the 2 θ range 10–50° with a step size of 0.02° at 2°/min. Diffractograms produced were analyzed using OriginPro 9.0.0.

Attenuated Total Reflection Fourier Transform Infrared Spectroscopy (ATR-FTIR). Characterization of fiber and physical mixture molecular structure were conducted using ATR-FTIR. Measurements were performed using a Bruker Vertex 90 spectrometer using the following parameters: resolution 4 cm⁻¹; scan count was 16 scans (also for background) over 4000–700 cm⁻¹ at ambient temperature (25 °C). Spectra were analyzed using Opus software version 7.2 and OriginPro 9.0.0.

Differential Scanning Calorimetry (DSC). All differential scanning calorimetry (DSC) studies were conducted on a TA Instruments Q2000 (New Castle, DE, USA) with a refrigerated cooling system attached at a dry nitrogen sample purge flow at 50 mL/min. Calibrations were performed using indium, *n*-octadecane, and tin; heat capacity constant calibration was performed using aluminum oxide TA sapphire disks at 2 °C/min with ±0.212 °C modulation amplitude over a 60 s period. All DSC experiments and calibrations were performed using a PerkinElmer 40 µL, 0.15 mm aluminum pan with an accompanying aluminum pinholed lid.

DSC experiments were performed on IBU starting material at 2 °C/min over an appropriate temperature range, while modulated temperature DSC (MTDSC) experiments were conducted on all other samples (i.e., K90F starting material, K90F fibers, and IBU-K90F PMs and fibers) at 2 °C/min with ±0.212 °C modulation amplitude over a 60 s period (over an appropriate temperature range). All experiments were conducted in triplicate. The data obtained was analyzed using the TA Instruments Universal Analysis 2000 software for Windows 2000/XP/Vista Version 4.7A.

Thermogravimetric Analysis (TGA). TGA studies were performed on a TA Instruments Hi-Res 2950 (New Castle, DE, USA) at a rate of 2 °C/min from 40 to 250 °C. All TGA experiments and calibrations were performed using a PerkinElmer 40 µL, 0.15 mm aluminum pan with an accompanying aluminum pinholed lid. All experiments were conducted in triplicate. The data obtained was analyzed using the TA Instruments Universal Analysis 2000 software for Windows 2000/XP/Vista Version 4.7A.

Thermogravimetric Analysis with Mass Spectroscopy (TGA-MS). Samples of K90F raw material, fibers, and IBU-K90F 10% PM and fibers were loaded onto aluminum T-zero pans and heated from 40 to 250 °C at a constant heating rate of 10 °C/min under a helium purge gas (50 mL/min) using a Discovery TGA (TA Instruments, USA). Evolved gas analysis was performed throughout the experiment using mass spectrometry, with data acquired in scan mode (*m/e* 5 to 70) using a Discovery MS mass spectrometer (New Castle, DE, USA). Data was analyzed using the TA Instruments Universal Analysis Software software for Windows 2000/XP/Vista Version 4.7A and OriginPro 9.0.0.

Loading, Solubility, and Release Studies. Calculation of IBU Content in Fibers. IBU content in the fibers generated was determined by dissolving 2 mg of fibers in ethanol. Solutions were then analyzed spectrophotometrically at 263 nm to assess the amounts of IBU in each sample. K90F did not interfere with the UV analysis.

Solubility Studies: 0.1 M Hydrochloric Acid (pH 1). Solubility studies were conducted on IBU dissolved in 0.1 M HCl and K90F solutions. Different amounts of K90F powders were dissolved in 0.1 M HCl to prepare K90F-HCl solutions with concentrations of 0.5%, 1%, 1.5%, and 2% w/v. Excess IBU was added to these solutions and vigorously stirred for 120 h at 37 °C ± 0.5 °C at 150 rpm. The saturated solutions were filtered using a 0.45 μm membrane, and the IBU concentration in the filtrate was determined spectrophotometrically at a wavelength of 263 nm. Each sample was measured in triplicate.

In Vitro Dissolution Studies. *In vitro* dissolution studies were conducted in a Copley dissolution bath (Copley Scientific, U.K.) (USP Apparatus 2) and in a shake incubator maintained at 37 ± 0.5 °C and a rotational speed of 50 rpm. Samples (starting material of IBU and IBU-K90F fibers) equivalent to 10 mg and 20 mg of IBU for sink and non-sink conditions respectively (based on the drug loading of each formulation) were used. Experiments were conducted in 10 mL (non-sink) and 900 mL (sink conditions) of 0.1 M HCl (pH 1). At predetermined intervals, a sample of the solution was withdrawn and filtered through a 0.45 μm filter, and the same amount of medium at the same temperature was replaced. Subsequently, the filtrate was analyzed spectrophotometrically at 263 nm. Experimental points were the average of at least three replicates.

The f_2 equation was used in this study to compare the dissolution performances under sink conditions between the IBU-K90F fibers generated and the starting IBU material. While this approach is primarily a regulatory tool, we use it here to evaluate the differences between profiles, given the potential for supersaturation which may complicate more usual methods such as initial rate assessment. The f_2 equation is a model that measures the similarity in percentage release between two dissolution profiles.²⁷ It is a logarithmic reciprocal square root transformation of the square error, which can be expressed by the following:

$$f_2 = 50 \times \log \left\{ \left[1 + \left(\frac{1}{n} \right) \times \sum_{t=1}^n (R_t - T_t)^2 \right]^{-0.5} \times 100 \right\} \quad (6)$$

where n is the number of time points, R_t is the percentage of drug release of a reference batch at the time t and T_t is the percentage of drug released at the comparison batch at time t (mean of at least 12 dosage units²⁸). When f_2 is greater than 50 (i.e., 50–100), this indicates the equivalence of both compared profiles; when f_2 is less than 50, this suggests that the profiles are different.

RESULTS

Drug–Polymer Miscibility. Miscibility can be defined as “the level of molecular mixing adequate to yield macroscopic properties expected of a single phase material (confirmed by the observation of a single glass transition temperature (T_g))”.²⁹ An estimation of drug–polymer miscibility in SDs is considered to be essential for the generation of physically stable SDs.³⁰ IBU-K90F miscibility was calculated using the Hansen solubility parameter (δ), which was calculated based on van Krevelen and Hoflyzer functional group contributions (eqs 3 and 4)²⁴ as described earlier. Compounds with similar δ values of $\Delta\delta < 7.0 \text{ MPa}^{1/2}$ are more likely to be miscible, whereas if $\Delta\delta > 10.0 \text{ MPa}^{1/2}$ compounds are likely to be

immiscible.²⁴ Our results showed that IBU (19.4 MPa^{1/2}) had a δ value lower than K90F (26.3 MPa^{1/2}). The $\Delta\delta$ between IBU and K90F is less than 7.0 MPa^{1/2} (i.e., 6.9 MPa^{1/2}), which indicates likely miscibility for the system. The calculated χ (eq 5) refers to the square of the difference in δ that were calculated from the values of functional group contributions at 25 °C as previously discussed. A value of χ close to zero suggests greater interaction between the drug and the polymer.²⁴ In this study, χ was calculated at 3.8, suggesting likely miscibility for the system. Table 1 provides a list of parameter values used to calculate the values outlined in eqs 3, 4, and 5.

Table 1. List of Parameter Values Used To Calculate Solubility Parameter Values As Outlined in Eqs 3, 4, and 5

	IBU	K90F
$\sum F_{di}/V$	17.9	20.4
$[(\sum F_{pi}^2)^{1/2}/V]^2$	2.2	13.7
$(\sum F_{hi})^{1/2}/V$	7.2	9.3
V_0	195.5	
$R (\text{J K}^{-1} \text{ mol}^{-1})$	8.3	
$T (\text{K})$	298.0	
$(\delta_{\text{drug}} - \delta_{\text{polymer}})^2$	48.0	

Characterization of Solution Parameters. Solution viscosity and surface tension are key determinants of fiber formation, with both parameters being dependent on concentration, molecular weight, and solute–solvent interactions.³¹

The measured values for solution viscosity and surface tension of K90F and IBU-K90F solutions are provided in Figure SI1. Viscosity and surface tension values for ethanol (at 25 °C) are 1.1 mPa s³² (obtained from ref 33) and 22.3 mN m⁻¹³⁴, respectively. Viscosity and surface tension measurements of K90F 10% w/v (in ethanol) solutions were 553.5 ± 25.2 mPa s and 36.9 ± 1.6 mN m⁻¹, respectively (represented as 0% w/v ibuprofen concentration in Figure SI1a,b). A decrease in viscosity was observed on increasing addition of IBU with the largest decrease observed with 50% drug loading. A systematic increase in solution surface tension was observed with increasing IBU concentration. The solution viscosity is related to several fiber morphological characteristics such as bead formation and fiber diameter changes, while surface tension is related to jet stability.¹⁰ High surface tension can also result in the formation of beads and beaded fibers.³⁵

Characterization of Fiber Diameter. SEM studies were conducted to observe changes in fiber morphology (in terms of surface appearance) and size as a function of increasing IBU concentration. Figure 2 shows SEM images of PG fibers generated using K90F and IBU-K90F 10%, 30%, and 50% w/v solutions with corresponding fiber diameter frequency diagrams. Although IBU-loaded fibers had the same morphology as unloaded fibers, they possessed larger diameters than K90F fibers (795.2 nm). IBU-K90F 10%, 30%, and 50% fibers had average diameters of 1.2 μm, 4.18 μm, and 5.4 μm (Figure 2). This trend of increased fiber diameter (from nano to micro range) upon addition of an additive such as a drug has been highlighted in the literature previously.^{36,37} The rotational speed influences the fiber length while the working pressure reduces the mean fiber diameter.^{14,18} A relatively low working pressure was used in this study; hence for future studies this could be increased to decrease the fiber diameter. IBU-K90F fibers did not show the presence of IBU crystals on the fiber

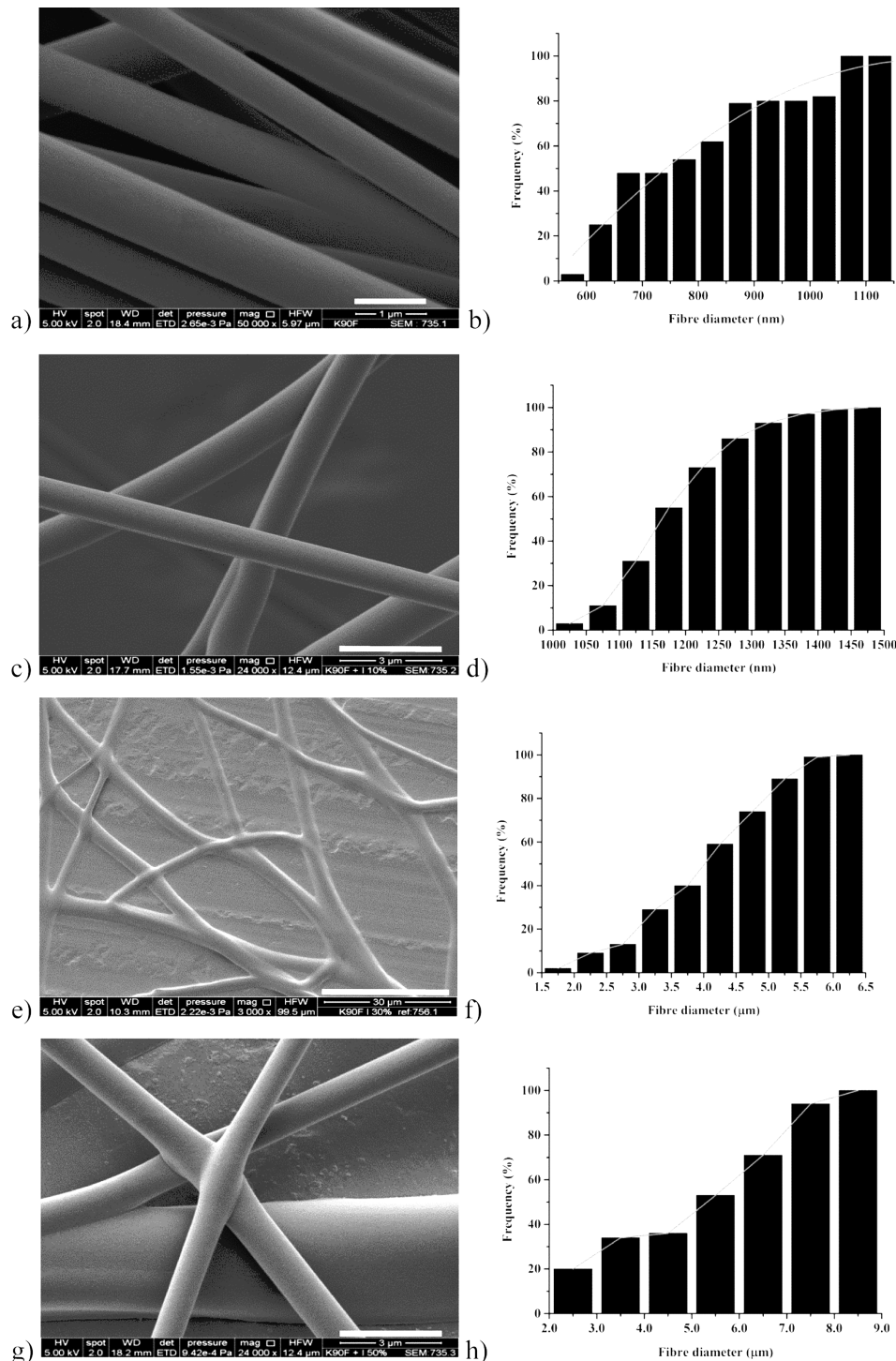


Figure 2. SEM images of (a) K90F \times 50,000 magnification, (b) corresponding fiber diameter frequency (cumulative %) distribution graph for K90F fibers, (c) IBU-K90F 10% fibers \times 24,000 magnification, (d) corresponding fiber diameter frequency (cumulative %) distribution graph for IBU-K90F 10% fibers, (e) IBU-K90F 30% fibers \times 3000 magnification, (f) corresponding fiber diameter frequency (cumulative %) distribution graph for IBU-K90F 30% fibers, (g) IBU-K90F 50% fibers \times 24,000 magnification, (h) corresponding fiber diameter frequency (cumulative %) distribution graph for IBU-K90F 50% fibers generated by PG.

surface in the systems studied. It should be noted that the changes in solution parameters (i.e., viscosity and surface tension) observed with increasing IBU concentration did not hinder fiber formation using this process. Furthermore, the interaction between the surface tension and the viscoelastic forces determines the formation of the smooth fibers.³⁵

Assessment of Fiber Amorphicity and Molecular Interactions. The diffraction pattern for IBU showed characteristic peaks of 2θ diffraction angles of $\sim 12^\circ$, $\sim 16^\circ$, and $\sim 22^\circ$ (Figure 3), while the diffraction pattern for K90F showed the expected amorphous halo (data not shown). Sharp peaks were absent in the diffraction patterns for K90F-IBU 10%, 30% (data not shown), and 50% fibers, suggesting that

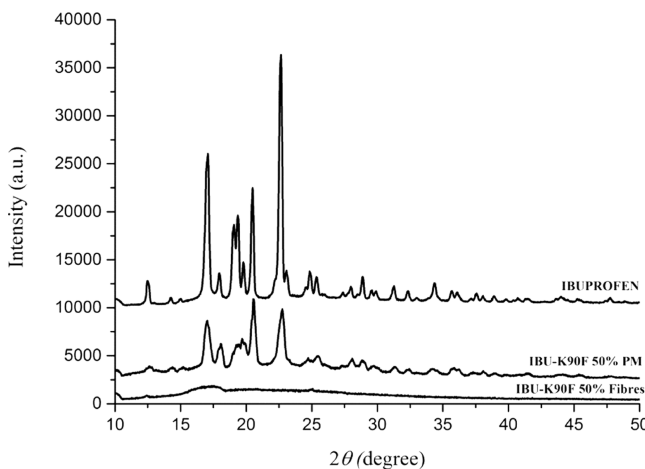


Figure 3. XRPD diffraction patterns for IBU and IBU-K90F 50% PMs and PG fibers.

IBU was present within the fiber in its amorphous form. In contrast, in the diffractograms of corresponding PMs all samples showed clear peaks corresponding to IBU, indicating the method to be sensitive to the detection of these levels of crystalline material. Figure 3 shows a representative XRPD diffraction pattern for IBU, IBU-K90F 50% PM, and PG fibers.

ATR-FTIR experiments were conducted on starting materials (IBU and K90F), IBU-K90F PMs, K90F PG fibers, and PG fibers to identify any differences in physical structure as well as evidence of molecular interaction by way of hydrogen bonding between IBU and K90F. Indications of strong hydrogen bonding between IBU and PVP have been reported in the carbonyl region ($\text{C}=\text{O}$ stretching) of IBU ($\sim 1700 \text{ cm}^{-1}$) and at the amide region (cyclic amide $\text{C}=\text{O}$ stretching) of K90F ($\sim 1666 \text{ cm}^{-1}$).^{38–40} Figure 4 shows ATR-FTIR spectra of IBU, K90F, IBU-K90F PMs, and PG fibers at the carbonyl region ($\text{C}=\text{O}$ stretching) of IBU and the amide region (cyclic amide $\text{C}=\text{O}$ stretching) of K90F. ATR-FTIR spectra of IBU-K90F 10% PM identified an irregularly shaped band overlapping between $\sim 1660 \text{ cm}^{-1}$ and 1700 cm^{-1} (both the cyclic amide of K90F and carbonyl region of IBU). With increasing IBU loading (i.e., IBU-K90F 10% and 30% PMs), a strong band was observed at 1708 cm^{-1} with a shoulder peak at $\sim 1650 \text{ cm}^{-1}$ which increased in intensity from 30% to 50% IBU loading. A strong single band occurring at 1648 cm^{-1} was observed in IBU-K90F 10% PG fibers. For IBU-K90F 30% and 50% PG fibers, two peaks were observed at $\sim 1655 \text{ cm}^{-1}$ (cyclic amide of K90F) and at 1708 cm^{-1} (carbonyl region of IBU). This peak appeared to increase in intensity with increasing IBU content. These results suggest an intermolecular interaction between IBU and K90F in IBU-K90F 10% PG fibers. In addition, with increasing IBU concentration (i.e., from 30% to 50% IBU loading) within PG fibers, a shifted peak at $\sim 1700 \text{ cm}^{-1}$ which possibly correlates to the carbonyl region of IBU was observed. Two peaks were observed in PM spectra confirming the absence of a molecular interaction between the two materials.

Literature evidence (using IR and carbon 13 nuclear magnetic resonance (^{13}C NMR)³⁸ and DSC⁴⁰) supports the occurrence of a solid-state interaction between IBU and PVP resulting in the formation of a stable glass-like form after storage. This interaction is thought to occur due to the formation of an intermolecular hydrogen bond between the free COOH group of IBU and the $\text{C}=\text{O}$ group of PVP.³⁸

Thermal Characterization of Fibers. Thermogravimetric Analysis (TGA) and TGA–Mass Spectroscopy (TGA–MS). It is well-known that amorphous materials may sorb water and other solvents, which may in turn profoundly influence their physical properties.^{41,42} TGA studies were conducted to measure solvent levels via weight change as a function of temperature for IBU, K90F, IBU-K90F PMs, and PG fibers. A general decrease in weight loss with increasing IBU loading was observed, though the weight loss was higher for IBU-K90F PG fibers (5.5–3.0% w/w) than PMs (3.2–2.4% w/v) (Table S1). This phenomenon has been observed previously^{43–48} and has been referred to as “hydrophobization of PVP” due to intermolecular interactions between IBU and K90F.

Further TGA studies were conducted on K90F (starting material and PG fibers), IBU-K90F 10% PM, and PG fibers using a TGA coupled to a mass spectrometer (MS) to identify the lost volatiles, given the mixed nature of the solvent used (ethanol and water). The mass-to-charge ratio (m/e) with the highest intensity for water and ethanol is 18 and 31 respectively. The change in ion current of these two species with increasing temperature was evaluated (Figure 5); the results confirm water loss but significantly also confirm the absence of any residual ethanol within K90F-IBU 10% PG fibers. These findings confirm that the solvent (i.e., ethanol) has been completely removed during fiber formation.

Modulated Temperature DSC. For amorphous SDs, it is expected that the drug–polymer interactions result in complete miscibility of the two components forming a single phase system;^{30,43,48} confirmation of this occurrence is the identification of a single T_g as well as the absence of XRPD diffraction peaks. While PG is a new polymeric fiber production method, the rapid solvent evaporation can reasonably be expected to result in amorphous system formation.⁴⁹ DSC and MTDSC data for IBU starting material saw a single endothermic response corresponding to the melt of IBU at 75.6°C (115.1 J g^{-1}) (data not shown) and T_g at -42.7°C (data not shown). MTDSC data for K90F starting material saw a T_g at 176.9°C , while K90F fibers had a T_g of 157.8°C .

MTDSC responses for IBU-K90F 10%, 30%, and 50% PG fibers did not show a melting peak of the IBU, but a single T_g was observed in all formulations at 147.7°C , 139.6°C , and 117.3°C respectively (Figure S12). These findings indicate that the system is indeed amorphous, with ibuprofen acting as a plasticizer.⁵⁰ It is important to note that PVP (a well-known hygroscopic polymer) based nanofibers could be expected to sorb a larger than expected amount of water due to not only the polymer’s hygroscopic nature but also the high surface-to-volume ratio properties of nanofibers. We associate the broad T_g responses observed here with simultaneous water loss, therefore, resulting in lower than expected T_g values for PG nanofibers (based on the Couchman–Karasz equation, a modification of the Gordon–Taylor relationship, e.g., IBU-K90F 10% PG fibers predicted T_g of 129.47°C).

In Vitro Dissolution Studies. The equilibrium solubility of crystalline IBU in 0.1 M HCl was measured as $95.6 \mu\text{g/mL}$. Solubility studies showed that with increasing K90F concentration (up to 2% w/v) IBU solubility increased 3-fold from $95.6 \mu\text{g/mL}$ to $380.4 \pm 3.7 \mu\text{g/mL}$ (Figure S13). We note that experimental determination of amorphous, as opposed to crystalline, solubility is known to be challenging due to the tendency of amorphous materials to rapidly crystallize upon contact with water.^{51,52} Nevertheless, the predicted amorphous solubility of IBU has been calculated by Sousa et al.⁵³ using

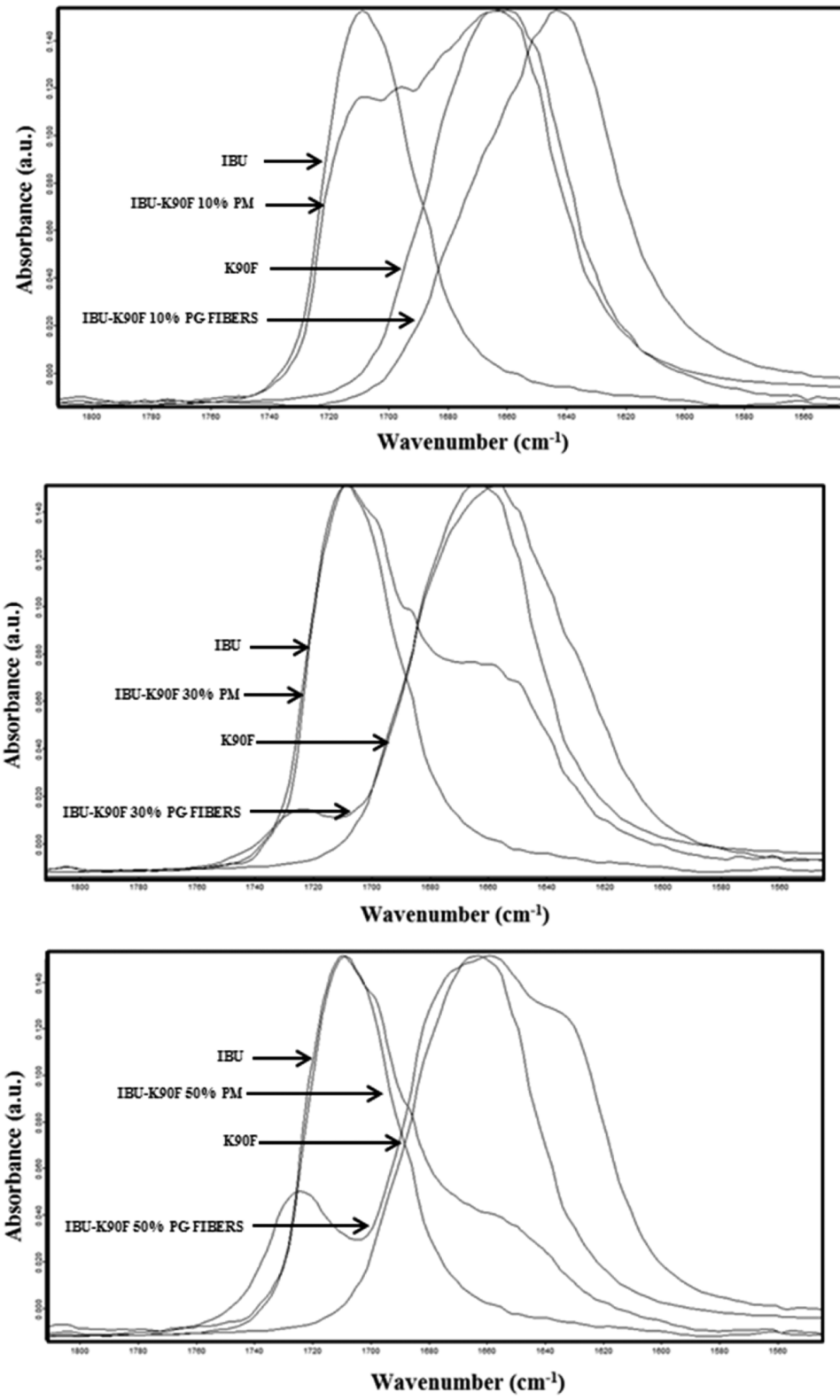


Figure 4. ATR-FTIR spectra IBU, K90F, and (a) IBU-K90F 10%, (b) IBU-K90F 30%, and (c) IBU-K90F 50% PG fibers and PMs at the carbonyl region (C=O stretching) of IBU and the amide region (cyclic amide C=O stretching) of K90F.

both a Hoffman (108.16 $\mu\text{g}/\text{mL}$) and heat capacity (C_p) (123.06 $\mu\text{g}/\text{mL}$) method; we include these figures here for comparison.

The drug content of all PG fibers was at 98.4–100.2% of the theoretical values. *In vitro* dissolution studies were conducted

under sink conditions in pH 1 to observe any dissolution rate enhancement achieved with IBU-K90F PG fibers compared to IBU starting material (Figure 6). An overall increase in the dissolution rate was observed in all IBU-K90F PG fiber formulations compared to IBU alone. T_{50} values for IBU, IBU-

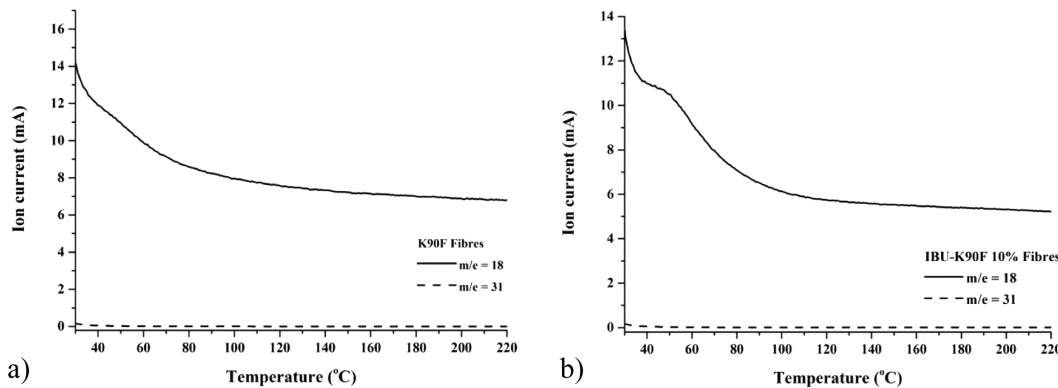


Figure 5. TGA-MS data for (a) K90F PG fibers and (b) IBU-K90F 10% PG fibers showing the ion current change on heating; the mass-to-charge ratio (*m/e*) with the highest intensity for water and ethanol is 18 and 31 respectively.

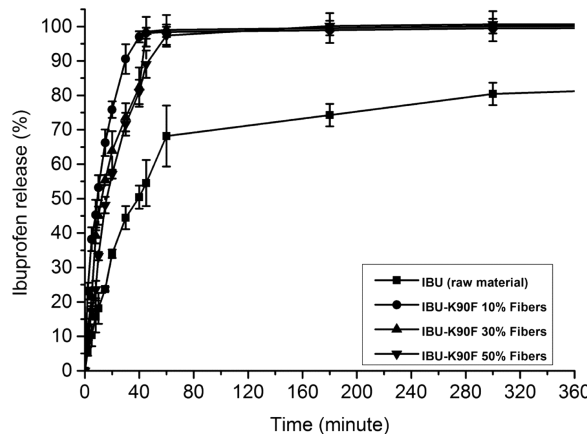


Figure 6. *In vitro* dissolution profile of IBU, IBU-K90F 10%, 30%, and 50% PG fibers conducted under sink conditions at pH 1 (0.1 M HCl).

K90F 10%, 30%, and 50% PG fibers were 40, 8, 14, and 16 min, respectively. Similarity factor (f_2) values (eq 6), which was used to compare the dissolution performances of IBU-K90F 10%, 30%, and 50% systems compared to IBU, were calculated at 23, 33, and 40 respectively. Values less than 50 suggest that the profiles differ, hence these profiles can be considered to be distinct from the drug alone.

Poorly soluble drugs in their stabilized amorphous form within an amorphous SD can generate a transient concentration significantly greater than the equilibrium saturation concentration of their crystalline counterparts.⁵⁴ Unfortunately, subsequent crystallization of the drug decreases the amorphous solubility advantage.⁵⁵ Nevertheless, drug supersaturation increases the driving force for oral absorption, and so maintaining an elevated and sustained level of drug supersaturation could be key to improve the bioavailability of poorly soluble drugs.⁵⁴ The inhibitory effect of polymers such as PVP (i.e., K90F) against crystallization of an amorphous drug is well documented in the literature.^{56,57} To observe the supersaturation effect of amorphous SDs, *in vitro* dissolution studies are usually conducted under non-sink conditions as is commonly encountered on entering the gastrointestinal (GI) tract.⁵⁴

The *in vitro* dissolution profile of IBU and IBU-K90F PG fibers obtained under non-sink conditions in pH 1 (Figure 7) saw an increase in the dissolution rate for IBU-K90F 10% PG fibers compared to IBU alone, while IBU-K90F 30% and 50% PG fibers saw a slower dissolution rate in comparison to this

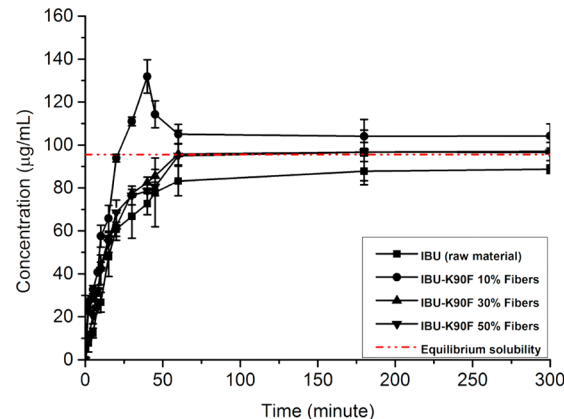


Figure 7. *In vitro* dissolution profile of IBU (raw material), IBU-K90F 10%, 30%, and 50% PG fibers conducted under non-sink conditions at pH 1 (0.1 M HCl).

composition. It is noted that dissolved PVP (i.e., K90F) is known to retard crystallization in supersaturation solutions.^{56,57} The supersaturation effect was only observed in IBU-K90F 10% PG fibers (statistically significant as $p < 0.05$ (Student's *t* test)), possibly because this formulation contained the highest content of K90F, and the inhibitory effect has been shown to increase with increasing polymer content.⁵⁶

DISCUSSION

The study has examined the feasibility of producing nanofibers of IBU in PVP (i.e., K90F) using the new approach of pressure gyration. The production process itself was extremely rapid, and scale up is clearly possible. While the use of such fibers for oral use is still at an early stage,^{12,13} it is clear that larger scale manufacture than is usually possible using, for example, electrospinning, is going to become a crucial consideration for commercialization, hence the results presented here are encouraging. Previous studies¹⁴ have explored the conditions required to manufacture PVP fibers, while here we see the effects of drug addition on the underpinning processing parameters and subsequent structure of the fibers, particularly in terms of diameter. More specifically, the fibers varied in diameter from the nanoscale to the micrometer scale on addition of IBU, this increase coinciding with changes to the viscosity and surface tension of the feed solutions. While nanofibers are usually generated with as low a diameter as possible, in this application it is not yet clear what the structural

requirements are likely to be in relation to performance (i.e., whether true nanoscale fibers are necessary for oral administration), plus there are several process parameters (such as working pressure and rotational speed) that may be changed to reduce the diameter still further. Solubility parameter studies predicted high miscibility between the IBU and K90F, which was supported by spectroscopic, thermal, and diffraction studies, which all indicated the generation of amorphous SDs; evidence was also obtained for a direct molecular interaction between the drug and polymer which may be expected to contribute to this good miscibility. A confounding issue that is inevitably associated with PVP, especially at these high surface areas, is the retention and sorption of solvents during processing and storage. Here we used TGA coupled with mass spectroscopy to demonstrate that the levels of residual ethanol were negligible, although further work may be required to optimize the water contents of these systems. Dissolution studies in sink conditions showed a marked increase in release rate compared to the drug alone which we suggest is due to a combination of the high surface area, the absence of the drug crystal lattice, and possibly the direct solubilization of the drug by the PVP, but interestingly under non-sink conditions the low drug loaded systems showed clear evidence of the “parachute” effect of supersaturation that is being commonly associated with enhanced absorption. Overall, therefore, the study has demonstrated that PG is a highly promising approach to the development of oral dosage forms from the viewpoint of both manufacturing feasibility and performance.

CONCLUSION

In this study the pressure gyration process was successfully used to prepare amorphous fibers of ibuprofen in PVP. The inclusion of ibuprofen was found not to impede fiber formation although a slightly higher diameter than the polymer alone was noted using the processing conditions utilized here. Thermal, spectroscopic, and diffraction studies indicated high miscibility (also predicted via solubility parameter calculations) and the generation of amorphous molecular dispersions. Spectroscopic studies also indicated a direct interaction between the drug and polymer, while TGA coupled with mass spectroscopy suggested that the ethanol in the mixed solvent used was driven off during processing but detectable water levels remained associated with the fibers. Dissolution studies showed a marked increase in release rate compared to the drug alone, with evidence found for supersaturation under non-sink conditions. Overall, the study has shown that both the production and performance of the nanofiber systems generated via pressure gyration show considerable promise as a novel approach to oral delivery of poorly water-soluble drugs.

ASSOCIATED CONTENT

Supporting Information

The Supporting Information is available free of charge on the ACS Publications website at DOI: [10.1021/acs.molpharmaceut.5b00127](https://doi.org/10.1021/acs.molpharmaceut.5b00127).

Characterization of solution parameters and thermal characterization of fibers ([PDF](#))

AUTHOR INFORMATION

Corresponding Author

*E-mail: duncan.craig@ucl.ac.uk.

Notes

The authors declare no competing financial interest.

ACKNOWLEDGMENTS

The authors would like to acknowledge the Engineering and Physical Sciences Research Council (EPSRC) for the funding of the work (EPSRC reference EP/L023059/1) and BASF and Astra Zeneca for their support of the project and supply of raw materials. In addition, the authors would like to thank David McCarthy (UCL School of Pharmacy) for his assistance with the FEIQuanta 200F field emission scanning electron microscope, Dr. Maria Fátima Pina, and Dr. Ziyi Yang.

REFERENCES

- (1) Chan, O. H.; Schmid, H.; Stilgenbauer, L.; Howson, W.; Horwell, D.; Stewart, B. Evaluation of a Targeted Prodrug Strategy to Enhance Oral Absorption of Poorly Water-Soluble Compounds. *Pharm. Res.* **1998**, *15* (7), 1012–1018.
- (2) Shiraki, K.; Takata, N.; Takano, R.; Hayashi, Y.; Terada, K. Dissolution Improvement and the Mechanism of the Improvement from Cocrystallization of Poorly Water-soluble Compounds. *Pharm. Res.* **2008**, *25* (11), 2581–2592.
- (3) Cheow, W. S.; Kiew, T. Y.; Hadinoto, K. Amorphous nanodrugs prepared by complexation with polysaccharides: Carrageenan versus dextran sulfate. *Carbohydr. Polym.* **2015**, *117* (0), 549–558.
- (4) Craig, D. Q. M.; Newton, J. M. Characterisation of polyethylene glycol solid dispersions using differential scanning calorimetry and solution calorimetry. *Int. J. Pharm.* **1991**, *76* (1–2), 17–24.
- (5) Craig, D. Q. M. The mechanisms of drug release from solid dispersions in water-soluble polymers. *Int. J. Pharm.* **2002**, *231* (2), 131–144.
- (6) Yang, Z.; Nollenberger, K.; Albers, J.; Craig, D.; Qi, S. Microstructure of an Immiscible Polymer Blend and Its Stabilization Effect on Amorphous Solid Dispersions. *Mol. Pharmaceutics* **2013**, *10* (7), 2767–2780.
- (7) Pina, M. F.; Zhao, M.; Pinto, J. F.; Sousa, J. J.; Craig, D. Q. M. The Influence of Drug Physical State on the Dissolution Enhancement of Solid Dispersions Prepared Via Hot-Melt Extrusion: A Case Study Using Olanzapine. *J. Pharm. Sci.* **2014**, *103* (4), 1214–1223.
- (8) Zhao, M.; Barker, S. A.; Belton, P. S.; McGregor, C.; Craig, D. Q. M. Development of fully amorphous dispersions of a low Tg drug via co-spray drying with hydrophilic polymers. *Eur. J. Pharm. Biopharm.* **2012**, *82* (3), 572–579.
- (9) Qi, S.; Moffat, J. G.; Yang, Z. Early Stage Phase Separation in Pharmaceutical Solid Dispersion Thin Films under High Humidity: Improved Spatial Understanding Using Probe-Based Thermal and Spectroscopic Nanocharacterization Methods. *Mol. Pharmaceutics* **2013**, *10* (3), 918–930.
- (10) Bhardwaj, N.; Kundu, S. C. Electrospinning: A fascinating fiber fabrication technique. *Biotechnol. Adv.* **2010**, *28* (3), 325–347.
- (11) Ignatious, F.; Sun, L.; Lee, C.-P.; Baldoni, J. Electrospun Nanofibers in Oral Drug Delivery. *Pharm. Res.* **2010**, *27* (4), 576–588.
- (12) Samprasisit, W.; Akkaramongkolporn, P.; Ngawhirunpat, T.; Rojanarata, T.; Kaomongkolgit, R.; Opanasopit, P. Fast releasing oral electrospun PVP/CD nanofiber mats of taste-masked meloxicam. *Int. J. Pharm.* **2015**, *487* (1–2), 213–222.
- (13) Malik, R.; Garg, T.; Goyal, A. K.; Rath, G. Polymeric nanofibers: targeted gastro-retentive drug delivery systems. *J. Drug Target.* **2015**, *23* (2), 109–124.
- (14) Mahalingam, S.; Edirisinghe, M. Forming of Polymer Nanofibers by a Pressurised Gyration Process. *Macromol. Rapid Commun.* **2013**, *34* (14), 1134–1139.
- (15) Luo, C. J.; Stoyanov, S. D.; Stride, E.; Pelan, E.; Edirisinghe, M. Electrospinning versus fibre production methods: from specifics to technological convergence. *Chem. Soc. Rev.* **2012**, *41* (13), 4708–4735.
- (16) Suryo, R.; Basaran, O. A. Dripping of a Liquid from a Tube in the Absence of Gravity. *Phys. Rev. Lett.* **2006**, *96* (3), 034504.

- (17) Weitz, R. T.; Harnau, L.; Rauschenbach, S.; Burghard, M.; Kern, K. Polymer nanofibers via nozzle-free centrifugal spinning. *Nano Lett.* **2008**, *8* (4), 1187–1191.
- (18) Raimi-Abraham, B. T.; Mahalingam, S.; Edirisinghe, M.; Craig, D. Q. M. Generation of poly(N-vinylpyrrolidone) nanofibres using pressurised gyration. *Mater. Sci. Eng., C* **2014**, *39* (0), 168–176.
- (19) Law, V.; Knox, C.; Djoumou, Y.; Jewison, T.; Guo, A. C.; Liu, Y.; Maciejewski, A.; Arndt, D.; Wilson, M.; Neveu, V.; Tang, A.; Gabriel, G.; Ly, C.; Adamjee, S.; Dame, Z. T.; Han, B.; Zhou, Y.; Wishart, D. S. DrugBank 4.0: shedding new light on drug metabolism. *Nucleic Acids Res.* **2014**, *42* (D1), D1091–D1097.
- (20) BASF. *Ibuprofen: Technical information*, 9th revised ed.; BASF: The Chemical Company: BASF SE Pharma Ingredients & Services: 67056 Ludwigshafen, Germany, 2010.
- (21) Buhler, V. *Kollidon: Polyvinylpyrrolidone excipients for the pharmaceutical industry*, 9th revised ed.; BASF: The Chemical Company: BASF SE Pharma Ingredients & Services: 67056 Ludwigshafen, Germany, 2008.
- (22) Hildebrand, J. H. *The Solubility of Non-Electrolytes*; Reinhold: New York, 1936.
- (23) Hansen, C. M.; Skaarup, K. Three-dimensional solubility parameter-key to paint component affinities. III. Independent calculation of the parameter components. *J. Paint Technol.* **1967**, *39* (511), 511–14.
- (24) Van Krevelen, D. W.; Te Nijenhuis, K., Chapter 7 - Cohesive Properties and Solubility. In *Properties of Polymers*, 4th ed.; Krevelen, D. W. V., Nijenhuis, K. T., Eds.; Elsevier: Amsterdam, 2009; pp 189–227.
- (25) Tian, Y.; Booth, J.; Meehan, E.; Jones, D. S.; Li, S.; Andrews, G. P. Construction of Drug–Polymer Thermodynamic Phase Diagrams Using Flory–Huggins Interaction Theory: Identifying the Relevance of Temperature and Drug Weight Fraction to Phase Separation within Solid Dispersions. *Mol. Pharmaceutics* **2013**, *10* (1), 236–248.
- (26) Koningsveld, R.; MacKnight, W. J. Liquid–liquid phase separation in multicomponent polymer systems. XXVII. Determination of the pair-interaction function for polymer blends. *Polym. Int.* **1997**, *44* (3), 356–364.
- (27) Moore, J. W.; Flanner, H. H. Mathematical comparison of dissolution profiles. *Pharm. Technol.* **1996**, *20* (6), 64–74.
- (28) O’Hara, T.; Dunne, A.; Butler, J.; Devane, J. A review of methods used to compare dissolution profile data. *Pharm. Sci. Technol. Today* **1998**, *1* (5), 214–223.
- (29) Mukerji, P. *Polymer-Polymer Miscibility*, Olagoke Olabisi, Lloyd M. Robeson, and Montgomery T. Shaw, Academic Press, New York, 1979, 370 pp. *J. Polym. Sci., Polym. Lett. Ed.* **1980**, *18* (8), 582–582.
- (30) Baird, J. A.; Taylor, L. S. Evaluation of amorphous solid dispersion properties using thermal analysis techniques. *Adv. Drug Delivery Rev.* **2012**, *64* (5), 396–421.
- (31) Bhattacharya, A.; Ray, P. Studies on surface tension of poly(vinyl alcohol): Effect of concentration, temperature, and addition of chaotropic agents. *J. Appl. Polym. Sci.* **2004**, *93* (1), 122–130.
- (32) Landolt-Börnstein, Viscosity and Diffusion. In *Properties of Matter in its Aggregated States*, 6th ed.; Springer-Verlag: Berlin, 1969; Vol. II.
- (33) 2.2.3 Viscosities. *Kaye & Laby Tables of Physical & Chemical Constants*, Version 1.1; 2008.
- (34) Vazquez, G.; Alvarez, E.; Navaza, J. M. Surface Tension of Alcohol Water + Water from 20 to 50.degree.C. *J. Chem. Eng. Data* **1995**, *40* (3), 611–614.
- (35) Mahalingam, S.; Ren, G. G.; Edirisinghe, M. J. Rheology and pressurised gyration of starch and starch-loaded poly(ethylene oxide). *Carbohydr. Polym.* **2014**, *114* (0), 279–287.
- (36) Katti, D. S.; Robinson, K. W.; Ko, F. K.; Laurencin, C. T. Bioresorbable nanofiber-based systems for wound healing and drug delivery: Optimization of fabrication parameters. *J. Biomed. Mater. Res.* **2004**, *70B* (2), 286–296.
- (37) Taepaiboon, P.; Rungsardthong, U.; Supaphol, P. Drug-loaded electrospun mats of poly(vinyl alcohol) fibres and their release characteristics of four model drugs. *Nanotechnology* **2006**, *17* (9), 2317–2329.
- (38) Sekizaki, H.; Danjo, K.; Eguchi, H.; Yonezawa, Y.; Sunada, H.; Otsuka, A. SOLID-STATE INTERACTION OF IBUPROFEN WITH POLYVINYL PYRROLIDONE. *Chem. Pharm. Bull.* **1995**, *43* (6), 988–993.
- (39) Bogdanova, S.; Pajeva, I.; Nikolova, P.; Tsakovska, I.; Müller, B. Interactions of Poly(vinylpyrrolidone) with Ibuprofen and Naproxen: Experimental and Modeling Studies. *Pharm. Res.* **2005**, *22* (5), 806–815.
- (40) Ivanov, I. T.; Tsokeva, Z. Effect of chirality on PVP/drug interaction within binary physical mixtures of ibuprofen, ketoprofen, and naproxen: A DSC study. *Chirality* **2009**, *21* (8), 719–727.
- (41) Zografi, G. STATES OF WATER ASSOCIATED WITH SOLIDS. *Drug Dev. Ind. Pharm.* **1988**, *14* (14), 1905–1926.
- (42) Ahlneck, C.; Zografi, G. THE MOLECULAR-BASIS OF MOISTURE EFFECTS ON THE PHYSICAL AND CHEMICAL-STABILITY OF DRUGS IN THE SOLID-STATE. *Int. J. Pharm.* **1990**, *62* (2–3), 87–95.
- (43) van Drooge, D. J.; Hinrichs, W. L. J.; Visser, M. R.; Frijlink, H. W. Characterization of the molecular distribution of drugs in glassy solid dispersions at the nano-meter scale, using differential scanning calorimetry and gravimetric water vapour sorption techniques. *Int. J. Pharm.* **2006**, *310* (1–2), 220–229.
- (44) Crowley, K. J.; Zografi, G. Water vapor absorption into amorphous hydrophobic drug/poly(vinylpyrrolidone) dispersions. *J. Pharm. Sci.* **2002**, *91* (10), 2150–2165.
- (45) Gordon, M.; Taylor, J. S. Ideal copolymers and the second-order transitions of synthetic rubbers. i. non-crystalline copolymers. *J. Appl. Chem.* **1952**, *2* (9), 493–500.
- (46) Imamura, K.; Fukushima, A.; Sakaura, K.; Sugita, T.; Sakiyama, T.; Nakanishi, K. Water sorption and glass transition behaviors of freeze-dried sucrose–dextran mixtures. *J. Pharm. Sci.* **2002**, *91* (10), 2175–2181.
- (47) López-Díez, E. C.; Bone, S. The interaction of trypsin with trehalose: an investigation of protein preservation mechanisms. *Biochim. Biophys. Acta, Gen. Subj.* **2004**, *1673* (3), 139–148.
- (48) Leuner, C.; Dressman, J. Improving drug solubility for oral delivery using solid dispersions. *Eur. J. Pharm. Biopharm.* **2000**, *50* (1), 47–60.
- (49) Yu, D.-G.; Branford-White, C.; White, K.; Li, X.-L.; Zhu, L.-M. Dissolution Improvement of Electrospun Nanofiber-Based Solid Dispersions for Acetaminophen. *AAPS PharmSciTech* **2010**, *11* (2), 809–817.
- (50) Gashi, Z.; Censi, R.; Malaj, L.; Gobetto, R.; Mozzicafreddo, M.; Angeletti, M.; Masic, A.; Di Martino, P. Differences in the interaction between aryl propionic acid derivatives and poly(vinylpyrrolidone) K30: A multi-methodological approach. *J. Pharm. Sci.* **2009**, *98* (11), 4216–4228.
- (51) Murdande, S. B.; Pikal, M. J.; Shanker, R. M.; Bogner, R. H. Solubility advantage of amorphous pharmaceuticals: I. A thermodynamic analysis. *J. Pharm. Sci.* **2010**, *99* (3), 1254–1264.
- (52) Hancock, B.; Parks, M. What is the True Solubility Advantage for Amorphous Pharmaceuticals? *Pharm. Res.* **2000**, *17* (4), 397–404.
- (53) Almeida e Sousa, L.; Reutzel-Edens, S. M.; Stephenson, G. A.; Taylor, L. S. Assessment of the Amorphous “Solubility” of a Group of Diverse Drugs Using New Experimental and Theoretical Approaches. *Mol. Pharmaceutics* **2015**, *12* (2), 484–495.
- (54) Sun, D. D.; Lee, P. I. Evolution of Supersaturation of Amorphous Pharmaceuticals: The Effect of Rate of Supersaturation Generation. *Mol. Pharmaceutics* **2013**, *10* (11), 4330–4346.
- (55) Van Eerdenbrugh, B.; Raina, S.; Hsieh, Y.-L.; Augustijns, P.; Taylor, L. Classification of the Crystallization Behavior of Amorphous Active Pharmaceutical Ingredients in Aqueous Environments. *Pharm. Res.* **2014**, *31* (4), 969–982.
- (56) Konno, H.; Handa, T.; Alonso, D. E.; Taylor, L. S. Effect of polymer type on the dissolution profile of amorphous solid dispersions containing felodipine. *Eur. J. Pharm. Biopharm.* **2008**, *70* (2), 493–499.

(57) Lindfors, L.; Forssén, S.; Westergren, J.; Olsson, U. Nucleation and crystal growth in supersaturated solutions of a model drug. *J. Colloid Interface Sci.* **2008**, *325* (2), 404–413.